Searching for Mirror Neutron Oscillations

Prajwal Mohanmurthy[1,a,b]
for PSI nEDM Collaboration
[a] Paul Scherrer Institute, Switzerland [b] ETH Zurich, Switzerland

1. Introduction

Baryogenesis requires baryon number violation. Neutron to mirror-neutron oscillation [0] is one such observable process. Two separate groups [2, 4] performed experiments in search of mirror-neutron oscillations and reported having found no evidence. The limit set on the oscillation time was $\tau_{nn'} > 448$s (90% C.L.) at mirror magnetic field, $B'_0 = 0$. Furthermore, it was shown that when the results of these two experiments were further analyzed [3,6,7], statistically significant signals for mirror-neutron oscillation in presence of a mirror magnetic field were found. The PSI nEDM collaboration performed a series of experiments to test these signals and the preliminary results are presented here.

General Techniques

There are two general techniques of searching for such oscillations:

1. Ultra Cold Neutron (UCN) storage experiment {where we search for magnetic field dependence of storage curves} and,
2. Regeneration Experiment {where a "particle through a wall" experiment is performed to look for a beam of cold neutrons regenerating across a barrier}.

Our attempt to search for mirror neutron oscillations employs technique # 1. The PSI nEDM collaboration made use of the PSI UCN source and a repurposed nEDM apparatus for this experiment.

How to setup the experiment?

- The most basic set of operations is called a cycle. The operations involved in a cycle are described in **Fig. 3** *(Right)*
- Each cycle has: 1. characteristic magnetic field – B_0 which was applied to the neutrons while they were stored in the storage vessel, 2. length of time the neutrons were stored – t^*_s before being counted.
- A cluster of cycles with the same characteristic B_0 & t^*_s is called a run. The run parameters are given in **Fig. 3** *(Top)*

Eq. 1 *(Bottom):* $\vec{B}$ is the magnetic field seen by SM particles, $\vec{B'}$ is the magnetic field experienced by mirror (SM') particles, β is the angle between $\vec{B}$ & $\vec{B'}$ and $\tau_{nn'}$ is the characteristic oscillation time.

$$P_{n\to n'}(t) = \frac{Sin^2\left(\frac{\mu B-\mu B'}{2}\right)t}{2\tau^2_{nn'}\left(\frac{\mu B-\mu B'}{2}\right)^2}[1+Cos(\beta)] + \frac{Sin^2\left(\frac{\mu B+\mu B'}{2}\right)t}{2\tau^2_{nn'}\left(\frac{\mu B+\mu B'}{2}\right)^2}[1-Cos(\beta)]$$

$$\mathcal{H} = \begin{bmatrix} \mu(\vec{\sigma}.\vec{B}) & 1/\tau_{nn'} \\ 1/\tau_{nn'} & \mu(\vec{\sigma}.\vec{B'}) \end{bmatrix}$$

[0] I. Yu. Kobzarev et al., Sov. J. Nucl. Phys. **3**, (1966) 837.
[1] G. Ban et al., Phys. Rev. Lett. **99** (2007) 161603.
[2] I. Altarev et al., Phys. Rev. D **80** (2009) 032003.
[3] Z. Berezhiani et al., EPJC **78** (2018) 717; [6] EPJC **72** (2012) 1974; [7] EPJC **64** (2009) 421.
[4] Serebrov, A. P. *et al.* PLB **663** (2008) 181-185; [5] NIMA **611**, (2009) 137–140.

VALUE (s)	CL%	DOCUMENT ID		TECN	COMMENT
>414	90	SEREBROV	08	CNTR	UCN, B field on & off
• • • We do not use the following data for averages, fits, limits, etc. • • •					
> 12	95	[29] ALTAREV	09A	CNTR	UCN, scan $0 \le B \le 12.5\ \mu T$
>103	95	BAN	07	CNTR	UCN, B field on & off

Tab. 1 Current standing constraints on $\tau_{nn'}$ from PDG.

2. Apparatus

Fig. 1 *(Left):* Schematic diagram of the PSI nEDM apparatus which was repurposed for this work. Notice the neutron polarizing magnet was turned off during this experiment. **Fig. 2** *(Bottom):* High current power supply used to achieve B_0 up to 25 μT.

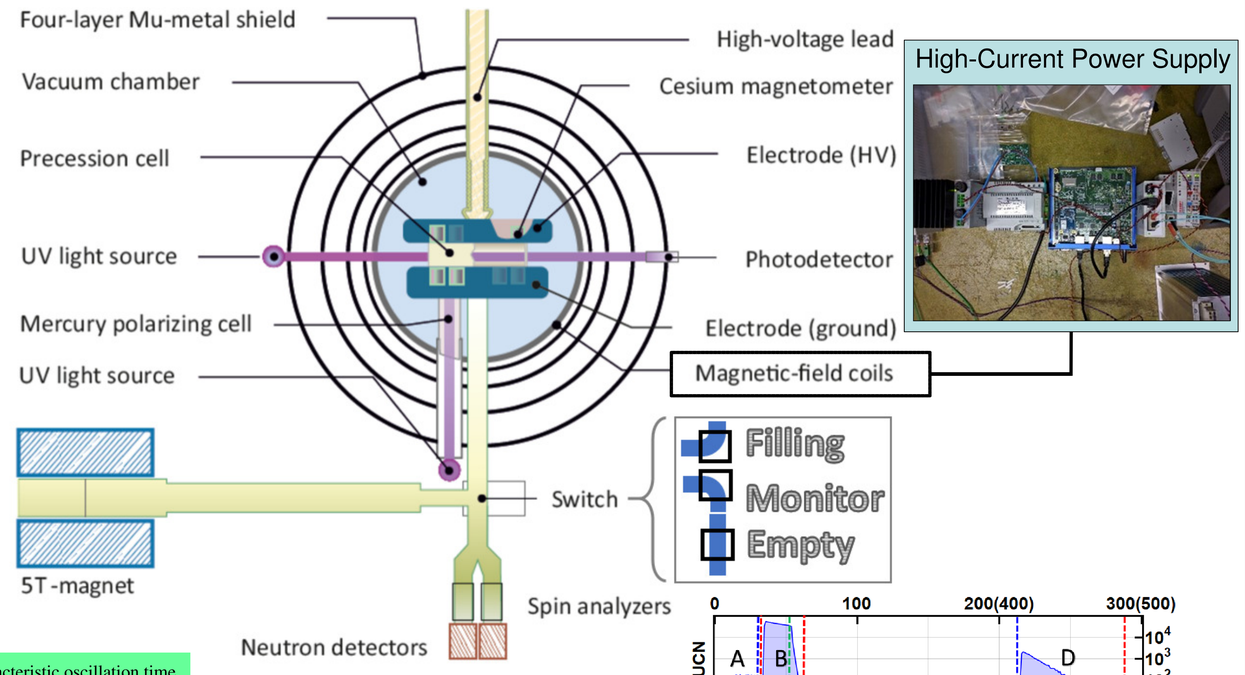

Application of Magnetic field – $\vec{B}$

$$N_\uparrow : +\vec{B}$$
$$N_\downarrow : -\vec{B}$$
$$N_0 : 0$$

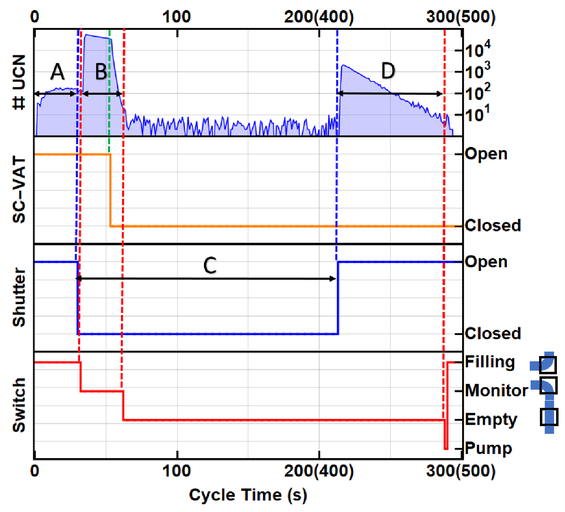

3. Schedule

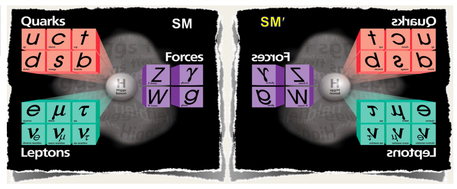

Fig. 3 (Clockwise) *(Top):* Run Plan. *(Right):* Cycle Plan. *(Bottom):* Procedure to gather neutron counting statistics.

Set $B_0 = 0$
Count $\{N_0^{Empty}(t_s), N_0^{Monitor}\}$

Set $B_0 = \pm\{10, 20\}$ μT
Count $\{N_{\uparrow,\downarrow}^{Empty}(t_s), N_{\uparrow,\downarrow}^{Monitor}\}$

Use normalized counts (to compensate for fluctuating initial number of neutrons stored):
$n_0 = N_0^{Empty}(t_s)/N_0^{Monitor}, n_{\uparrow,\downarrow} = N_{\uparrow,\downarrow}^{Empty}(t_s)/N_{\uparrow,\downarrow}^{Monitor}$

4.a. Analysis Technique

$B' = 0$

Fig. 4 Example distribution of $n_\uparrow(B = 10\mu T, t^*_s = 380s)$

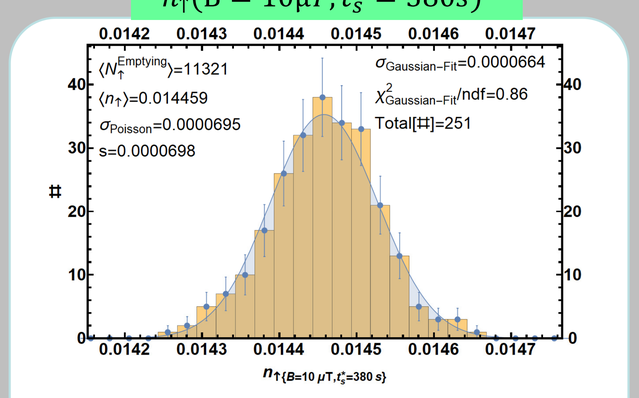

$$\langle E_B\rangle = \frac{2\langle n_0\rangle}{\langle n_\uparrow\rangle+\langle n_\downarrow\rangle} - 1\ ;\ \langle A_B\rangle = \frac{\langle n_\uparrow\rangle-\langle n_\downarrow\rangle}{\langle n_\uparrow\rangle+\langle n_\downarrow\rangle}$$

The neutron counting distributions are then combined with the time of flight spectra.

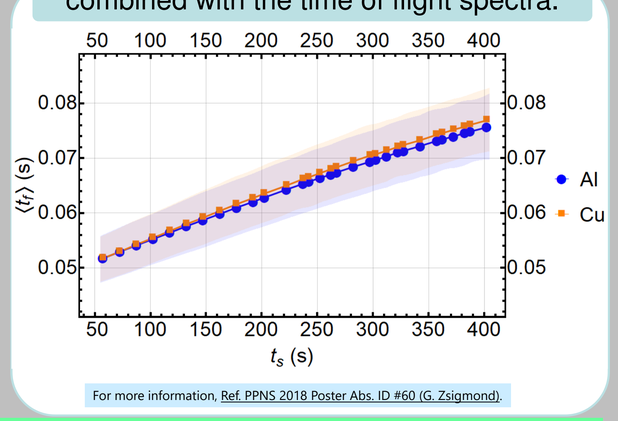

Fig. 5 Plot showing the spectral variation of the uncertainty in mean time between two consecutive collisions - $\{t_f\}$ with time of UCN storage - $\{t_s\}$. Mean value here comes from averaging over the path history of the trajectory of the UCNs in the storage vessel, and over the uncertainty in the energy spectrum of the stored UCNs. The error bars show the error on the mean.

Fig. 6 Combining **Fig. 4** & **Fig. 5** gives a central value and a normal error associated with each run.

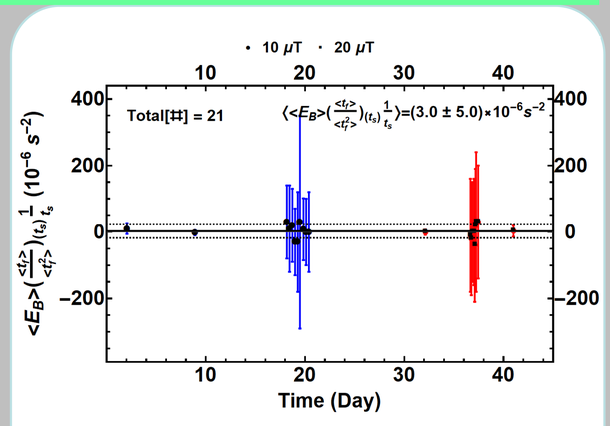

Obtain the distribution of the oscillation time, '$\tau_{nn'}$'.

Eq. 2

$$\tau^2_{nn'} = \sqrt{\frac{t_s}{\langle t_f^2\rangle}\frac{\langle t_f\rangle}{-\langle E_B\rangle}}$$

$$-1/\Delta_0$$

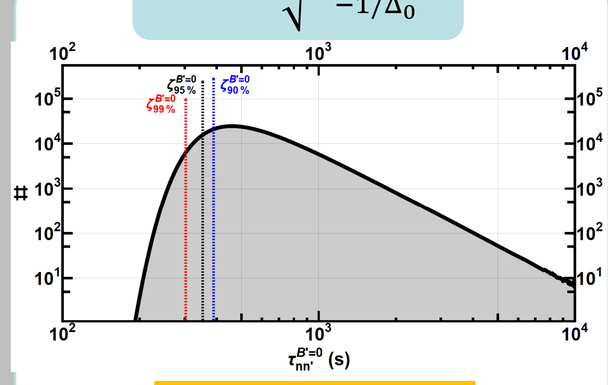

$$\tau^{(B'=0,\,95\%\,C.L.)}_{nn'} > 352\ s$$

Fig. 7 : Plot Showing the distribution of the $n-n'$ oscillation time, '$\tau_{nn'}$', under the assumption of $B' = 0$.

4.b. Analysis Technique

For the case where we do not assume $B' = 0$, we follow the same recipe set forth in **Fig. 4** → **Fig. 7**. The difference being that the final cumulative constraint on $\tau_{nn'}$ is dependent on B' according to **Eqs. 3 & 4**. Here we present the constraint which has been achieved with the amount of statistics collected.

Eq. 3 – 4 Here, $\omega' = \gamma' B'/4$, $\omega = \gamma B/4$, and $\eta = B/B'$

$$\tau^{B'\neq 0,E_B}_{nn'} = \sqrt{\underbrace{\frac{t_s}{\langle t_f\rangle\langle E_B\rangle}}_{1/\Delta_B}\underbrace{\frac{\eta^2(3-\eta^2)}{2\omega'^2(1-\eta^2)^2}}_{f_{E_B}(\eta)}}$$

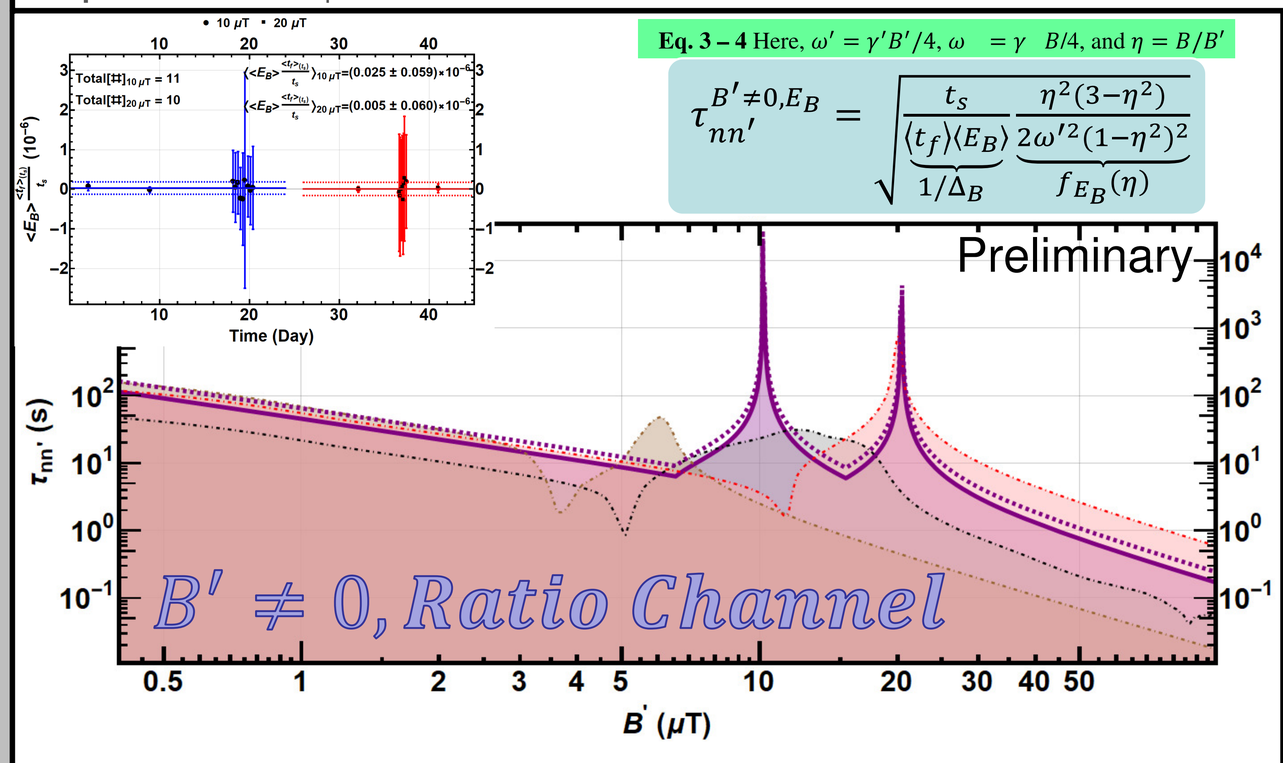

Fig. 8 Solid purple curve: *this work; dashed purple curve: *this analysis - energy spectrum uncertainties neglected; dot-dashed black curve: [3]; dot-dashed brown curve: [1]; dot-dashed red curve: [5].

$$\frac{\tau^{B'\neq 0,A_B}_{nn'}}{\sqrt{\cos\beta}} = \sqrt{\underbrace{\frac{t_s}{\langle t_f\rangle\langle A_B\rangle}}_{1/D_B}\underbrace{\frac{\eta^3}{\omega^2(1-\eta^2)^2}}_{f_{A_B}(\eta)}}$$

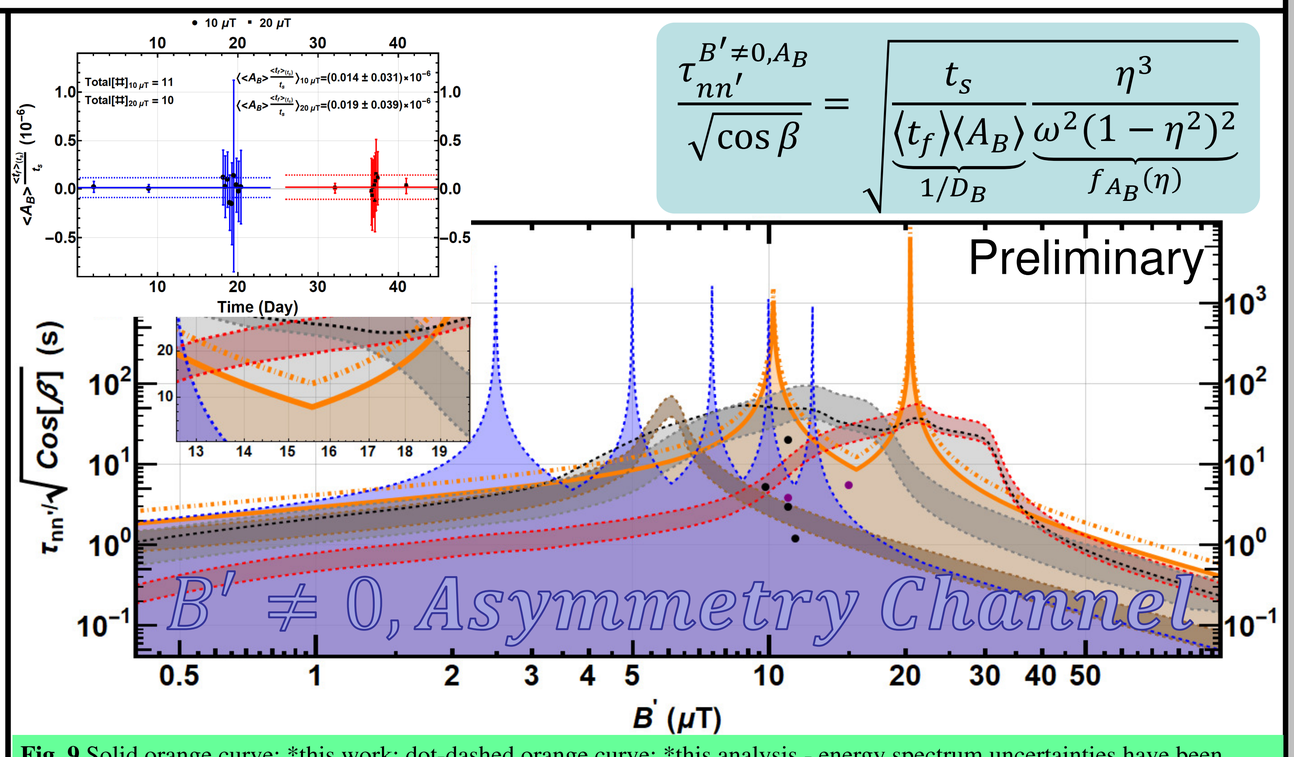

Fig. 9 Solid orange curve: *this work; dot-dashed orange curve: *this analysis - energy spectrum uncertainties have been neglected; dashed black curve: [3]; dashed blue curve: [2]; red region & dashed red lines: 5.2σ anomaly [5], [6]; brown region & dashed brown lines: 3σ anomaly in [1]; gray region & dashed gray lines: 2.5σ anomaly in B2 series [3]; purple dots: signal in [7]; black dots: signal in [6].

5. Summary

This effort excludes signals in the range $B' < 4\ \mu T$ and $B' > 37\ \mu T$. This is the best limit around $B' \sim 10\ \mu T$ and $B' \sim 20\ \mu T$. Sidereal and annual modulation limits are not as good as the ones here. Signals in the range $B' \in (4,37)\mu T$ have not been excluded, and future searches must focus efforts here.

[1] prajwal@mohanmurthy.com

* This work was supported by SERI FCS # 2015.0594 and Sigma Xi Grant # G2017100190747806